Phys Chem Minerals (2008) 35:249–257
DOI 10.1007/s00269-008-0218-6

ORIGINAL PAPER

In situ strength measurements on natural upper-mantle minerals

Junji Yamamoto · Jun-ichi Ando · Hiroyuki Kagi · Toru Inoue · Akihiro Yamada · Daisuke Yamazaki · Tetsuo Irifune

Received: 20 August 2007 / Accepted: 18 January 2008 / Published online: 20 February 2008

Abstract Using in situ strength measurements at pressures up to 10 GPa and at room temperature, 400, 600, and 700°C, we examined rheological properties of olivine, orthopyroxene, and chromian-spinel contained in a mantle-derived xenolith. Mineral strengths were estimated using widths of X-ray diffraction peaks as a function of pressure, temperature, and time. Differential stresses of all minerals increase with increasing pressure, but they decrease with increasing temperature because of elastic strain on compression and stress relaxation during heating. During compression at room temperature, all minerals deform plastically at differential stress of 4–6 GPa. During subsequent heating, thermally induced yielding is observed in olivine at 600°C. Neither orthopyroxene nor spinel shows complete stress relaxation, but both retain some stress even at 700°C. The strength of the minerals decreases in the order of chromian-spinel ≈ orthopyroxene > olivine for these conditions. This order of strength is consistent with the residual pressure of fluid inclusions in mantle xenoliths.

Keywords Rheology · X-ray diffraction measurement · Mantle mineral · Fluid inclusion · Geobarometry

J. Yamamoto (✉)
Woods Hole Oceanographic Institution,
Woods Hole, MA 02543, USA
e-mail: jyamamoto@whoi.edu; jyamac@mac.com

J. Yamamoto
Institute for Geothermal Sciences, Graduate School of Science,
Kyoto University, Beppu 874-0903, Japan

J. Ando
Department of Earth and Planetary Systems Science,
Graduate School of Science, Hiroshima University,
Kagami-yama 1-3-1, Higashi-Hiroshima 739-8526, Japan

H. Kagi
Geochemical Laboratory, Graduate School of Science,
The University of Tokyo, Hongo, Tokyo 113-0033, Japan

Present Address:
A. Yamada
Department of Geology, University of California Davis,
One Shields Avenue, Davis, CA 95616, USA

T. Inoue · A. Yamada · D. Yamazaki · T. Irifune
Geodynamics Research Center, Ehime University,
2-5 Bunkyo-cho, Matsuyama 790-8577, Japan

D. Yamazaki
Institute for Study of the Earth's Interior, Okayama University,
Yamada 827, Misasa 682-0193, Japan

Introduction

Pressure inside fluid inclusions in mantle xenoliths supports estimation of the original depth at which the xenoliths were entrained by host magma (e.g., Roedder 1965; Yamamoto et al. 2002, 2007). Even in the same xenolith, however, fluid inclusions show different internal pressures. The pressure amplitudes correspond to those of surrounding minerals, such as in the order of chromian-spinel (spinel) ≥ orthopyroxene ≈ clinopyroxene >> olivine (De Vivo et al. 1988; Schwab and Freisleben 1988; Frezzotti et al. 1992; Yamamoto et al. 2002, 2007; Sapienza et al. 2005), perhaps because of depressurization of xenoliths during transportation to shallower regions of the Earth. The pressure applied to the xenoliths decreases during depressurization, whereas the pressure inside the fluid inclusion remains constant, which leads to differential pressures in the xenoliths. They plastically deform the lattice surrounding the fluid inclusion. Therefore, the internal pressure of a fluid inclusion in a soft mineral should

decrease more than that in a hard mineral. The volume change of the fluid inclusion in a mantle xenolith during ascent to the Earth's surface can be calculated using the 'constitutive equation' with data of rheological properties of olivine (Karato and Jung 2003; Hirth and Kohlstedt 2003), pyroxene (Mackwell 1991), and spinel (Mitchell et al. 1976). Figure 1 presents strain rates of major mantle minerals as a function of temperature. Because several parameters for olivine used in the calculation were obtained from natural olivine, whose major element composition resembles that of typical mantle olivine, it is reasonable to infer that mantle olivine deforms plastically by a strain rate of ca. 1×10^{-7} s^{-1} at 1,000°C and differential stress of 1 GPa. If a fluid inclusion in a mantle xenolith has excess pressure greater than 1 GPa, the crystal lattice of olivine surrounding the fluid inclusion deforms by the strain rate. Then the fluid inclusion volume expands by 10% for about 3 days. The lower residual pressure of fluid inclusions in olivine in mantle xenoliths is attributable to selective plastic deformation of the crystal lattice of olivine surrounding the fluid inclusion. There is, however, no conclusive evidence that residual pressure of the fluid inclusion in the other mineral species (pyroxene or chromian-spinel) is adequate for a geobarometer. The rheological properties were often determined using samples, which are not derived directly from mantle. Such samples have different chemical conditions from mantle rocks, for example, major element composition, oxygen fugacity and water content. As might be apparent from Fig. 1, strength on plastic deformation of orthopyroxene is closely related to the major element composition. Experimental constraints for rheological properties of natural mantle minerals are necessary to understand the mechanism of deformation of mantle minerals.

Studies by Weidner et al. (1994, 1998) and Weidner (1998) utilized an experimental technique using high-pressure apparatus and synchrotron radiation, which can obtain quantitative data of elastic and plastic behavior of samples at in situ high-pressure conditions. This technique emphasizes the peak shapes of X-ray diffraction lines from powder samples. Chen et al. (1998, 2002) and Zhang et al. (2002) applied this technique to elucidate the yield strength and plastic behavior of mantle minerals and moissanite. Applying this technique to natural mineral samples from a mantle xenolith, we report the relative strengths of natural mantle minerals such as olivine, orthopyroxene and spinel at high-pressure and high-temperature conditions. The strengths of plastic deformations of mantle minerals are related closely to their respective chemical compositions (e.g., Saxena et al. 1993). For that reason, it is important to perform strength measurements on natural mantle minerals. We analyzed stress relaxation of two natural mantle minerals simultaneously using multi-capsule assembly.

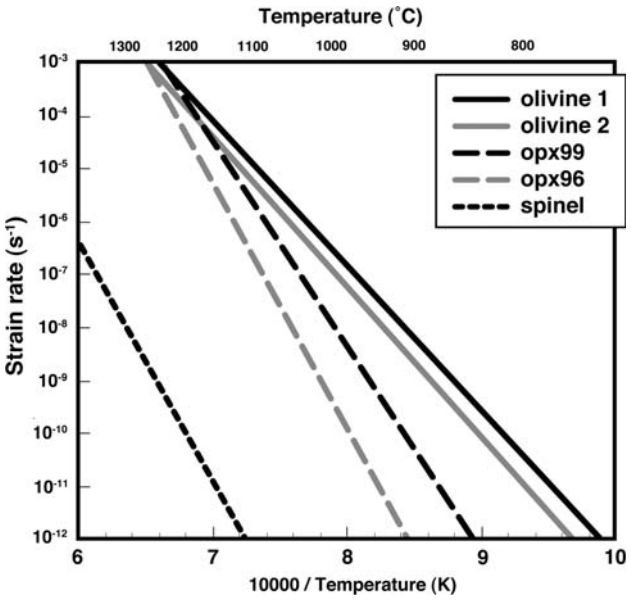

Fig. 1 Calculated Arrhenius diagram of the strain rate versus 1/T for olivine, orthopyroxene, and spinel. Data sources of rheological parameters are as follows: olivine [olivine 1 (Mg# [100 × Mg/(Mg + Fe)] = 90) from Karato and Jung (2003), olivine 2 (Mg# = 91) from Hirth and Kohlstedt (2003)], orthopyroxene (opx99 and opx96 from Mackwell (1991), whose respective Mg# are 99 and 96), and spinel [spinel ($MgAl_2O_4$) from Mitchell et al. (1976)]

This technique allowed direct comparison of strength of the natural mantle minerals at exactly same pressure and temperature condition. Based on rheological properties of natural mantle minerals obtained in this study, we clarify the reasons why fluid inclusions in mantle xenoliths show densities that are specific to individual host mineral species.

Samples

The studied samples are olivine, orthopyroxene, and spinel, which constituted a spinel-lherzolite. This spinel-lherzolite is a mantle-derived xenolith collected from Ennokentiev, in the middle of the Sikhote-Alin region of far eastern Russia. This xenolith exhibits a protogranular texture and consists mainly of olivine, orthopyroxene, and clinopyroxene, with lesser amounts of spinel. The average grain diameter of these minerals is about 0.5 mm. The Mg# [100 × Mg/(Mg + Fe)] of olivine and the Cr# [Cr/(Cr + Al)] of spinel are, respectively, 88 and 0.12 (Table 1), whose values are within the typical compositions of mantle rocks. These constituent minerals contain many fluid inclusions filled with CO_2. The oxygen fugacity around the CO_2 fluid inclusion is restricted to around QFM+2.0 in log unit by a chemical equilibrium between CO and CO_2. No other components such as CH_4 and H_2O were detected from fluid inclusions (Yamamoto et al. 2002, 2004). Micro-Raman

Table 1 Average core compositions (wt.%) of minerals in a ultramafic xenolith from far eastern Russia

Sample locality rock type mineral	En-1 Ennokentiev lherzolite			
	Olivine	opx	cpx	Spinel
Mg#	88.42	88.84	89.28	73.38
Cr#				0.12
SiO_2	39.86	54.37	51.78	0.05
TiO_2	0.02	0.11	0.51	0.20
Al_2O_3	0.19	4.57	6.77	55.54
Cr_2O_3	0.00	0.31	0.73	11.56
FeO	11.22	7.23	3.16	12.64
MnO	0.14	0.13	0.08	0.01
MgO	48.10	32.30	14.75	19.55
CaO	0.06	0.71	20.17	0.00
Na_2O	0.01	0.15	1.86	0.00
K_2O	0.01	0.01	0.01	0.01
NiO	0.38	0.10	0.04	0.39
P_2O_5	0.00	0.00	0.10	0.00
V_2O_3	0.01	0.01	0.04	0.05
Total	100	100	100	100
T (°C)				912

Equilibrium temperature (T) was estimated using the two-pyroxene geothermometer described in Wells (1977)

opx orthopyroxene, *cpx* clinopyroxene

spectroscopic analyses of CO_2-dominant fluid inclusions in mantle minerals enables elucidation of the depth (or pressure) at which the xenoliths are trapped by host magma (Yamamoto et al. 2002, 2007; Hirano et al. 2004) and indicates that the present xenolith is of the uppermost mantle-origin from 0.96 to 1.04 GPa pressure corresponding depth of 35–37 km, assuming that the crustal thickness and densities of crustal and mantle rocks are 34 km, 2.85 and 3.30 g/cm^3, respectively (Yamamoto et al. 2002).

Experimental method

Strain and stress measurement techniques for minerals at in situ high-pressure conditions using high-pressure apparatus and synchrotron radiation have been summarized by Weidner et al. (1994, 1998) and Weidner (1998). In this method, deviatoric stress is generated by compression of powder sample owing to the void space between grains and the point contacts of the grains. The strength of the sample reflects the magnitude of the generated deviatoric stress. This microscopic stress results in the broadening of the X-ray diffraction peaks caused by the elastic strain of grains. During the temperature increase, narrowing of the X-ray diffraction peaks occurs as the stress relaxes because of plastic deformation of the grains. Therefore, rheological information can be derived from the quantification of this process.

As summarized by Weidner et al. (1994) and Zhang et al. (2002), the width of the diffraction lines is a convolution of the instrument response, sample response function, and the longitudinal elastic strain parallel to the diffraction vector. By assuming that a spectrum observed at room temperature and pressure includes the first two of these, the strain is calculable using the following equation.

$$\varepsilon = (1/E)\left[W_0(E)^2 - W_{\mathrm{i}}(E)^2\right]^{1/2} \quad (1)$$

In that equation, E is the X-ray photon energy, W_0 is the observed peak width measured on the energy scale at a given experimental condition, and W_{i} is the instrumental contribution.

Strain measurements were performed using a Kawai-type multi-anvil high-pressure apparatus (SPEED-1500) installed at the beamline BL04B1, SPring 8. Energy-dispersive X-ray diffraction data were collected using a solid state Ge detector and a receiving slit of $\sim$50 μm at a fixed angle of 2θ, around 5° (Utsumi et al. 1998; Irifune 2002). The energy scale of the detector was calibrated using characteristic X-rays of Kα lines of Cu, Mo, Ag, Ta, Pt, Au, and Pb. Figure 2 shows the cell assembly of the present high-pressure experiments. Mo and graphite were used respectively as the electrode and furnace. The pressure medium comprised $LaCrO_3$, (Mg, Co)O, hexagonal BN (hBN), and zirconia. To increase the X-ray transparency, we put a boron rod on the central (Mg, Co)O pressure medium. Using an agate mortar, olivine, orthopyroxene, and spinel were separated carefully from the spinel-lherzolite and were crushed into a fine powder with grain size of less than 1 μm. Two sets of powder samples can be loaded symmetrically: the pair of olivine-orthopyroxene or olivine-spinel put into the hBN sleeve. This sample configuration enables the simultaneous comparison of strains of two minerals using the same pressure and temperature conditions. The pressure standard was NaCl, which was set into the center of the cell; pressures were calculated from Decker's equation of state for NaCl (Decker 1971). Temperature was measured using a $W_{97}Re_3$–$W_{75}Re_{25}$ thermocouple, whose hot junction was positioned at the center of the furnace. It was in direct contact with the pressure standard. No correction was applied for the effect of pressure on the thermocouple electromotive force.

The sample was compressed first gradually up to ca. 10 GPa at room temperature for more than 6 h. X-ray diffraction patterns were recorded at 1 GPa intervals during compression. Subsequently, the sample was heated stepwise at 400, 600, and 700°C at a constant pressure load. X-ray diffraction patterns were recorded at each temperature as a function of heating time to characterize the stress relaxation.

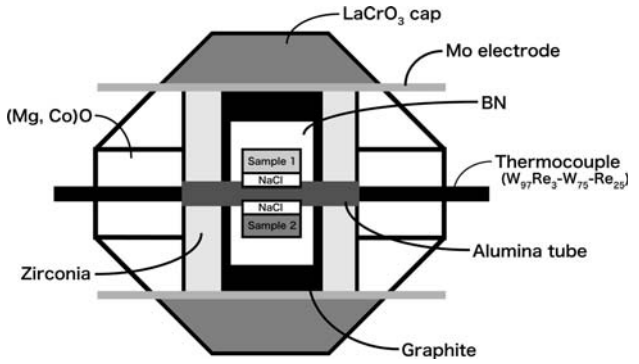

Fig. 2 Schematic cross section of a cell assembly with an 8-mm truncated edge length (TEL). Boron windows were placed vertically to the cross section

Data were collected continually at intervals of 50 s for the first 40 min, and subsequently at intervals of 300 s for each temperature. The stresses generated in the samples were estimated from FWHM (Full Width Half Maximum) of some diffraction peaks from the samples located at in situ high-temperature and high-pressure conditions.

Results and discussion

Figure 3 shows the obtained X-ray diffraction peaks of the samples at various conditions. Diffraction patterns of high-temperature were taken at 1,000 s after the temperature reached the indicated value (Fig. 3). With increasing pressure to 10 GPa at room temperature, the peak width of all samples broadened two to three times compared to the width at room temperature and pressure. No phase transition was observed throughout the experiments in all samples. Orthopyroxene is probably in a metastable state at the condition of 10 GPa; for example, clinoenstatite is stable at conditions of 700°C and 10 GPa (e.g., Ulmer and Stalder 2001). All diffraction peaks are, however, indexed by inherent peaks of orthopyroxene (Fig. 3b), which might be caused by sluggish transformation. The diffraction peak (420) of orthopyroxene broadened asymmetrically on the compression. This might result from the occurrence of the peak (221) with d spacing of 3.197 Å (Fig. 3b). However, it has no serious effect on the present study because there is no substantial rise in intensity of the peak (221) during compression.

Peak broadening can result from strain heterogeneity associated with deviatoric stress and small grain size. As described in Gerward et al. (1976), a general form of Eq. (1) is given as

$$W_0^2 - W_i^2 = W_d^2 + (\varepsilon E)^2, \quad (2)$$

where W_d is the contribution of the sample grain size to the peak-width broadening. Figure 4 shows the peak

Fig. 3 Diffraction patterns of **a** olivine, **b** orthopyroxene, and **c** spinel at the indicated temperature and pressure conditions. The patterns of high-temperatures were collected at 1,000 s at each temperature. Indexed peaks were used for estimation of the contributions of the grain size to peak broadening and differential stress of samples shown in Figs. 4 and 5

broadening ($W_0^2 - W_i^2$) against energy squared for several peaks. We noted that (420) peak of orthopyroxene is not included in this diagram in order to prevent possible interference from the peak (221). The data can be fitted using straight lines with $W_d^2 = 0$. An intercept near zero indicates the slight contribution of the small grain size of the sample to peak broadening. The observed peak broadening is therefore a result of strain. Some planes start to yield beyond 3 GPa. For that reason, we did not apply data of more than 3 GPa. Orthopyroxene shows a negative slope for 0.8 GPa, which indicates that the square of peak broadening has an uncertainty of ca. 0.2 [kev^2].

Differential stresses can be estimated using Hooke's law. For estimation, we adopted appropriate aggregate Young's modulus at room temperature and pressure, which are 181.7 GPa for orthopyroxene (Kung et al. 2004), and 195.0 and 277.0 GPa for olivine and spinel (Anderson and Isaak 1995). Temperature dependence of the Young's modulus was considered using temperature derivatives of elastic modulus for orthopyroxene (Bass, 1995), and olivine and spinel (Anderson and Isaak 1995). Regarding pressure dependence, pressure derivatives proposed by Bass (1995) were used for all minerals. Figure 5 shows the differential stress as a function of load pressure followed by heating at the constant load. The differential stresses of all samples almost increase with increasing pressure, and then decrease with increasing temperature. Under compression, the stresses for olivine increase with pressure up to ca. 4 GPa. At higher pressures, the stresses for olivine saturate and remain approximately constant with further loading to 10 GPa (see Fig. 5a, b). The increasing rate of stress in orthopyroxene and spinel with pressure decreases drastically at the differential stress of ca. 4 GPa. This fact indicates that the differential stress exceeds the yield strength of the samples at 4–6 GPa, as with olivine. They have begun to deform plastically. The yield strength calculated from (130) and (222) peaks of olivine is around 4 GPa, which is almost the same as that of anhydrous olivine, as presented by Chen et al. (1998) and Raterron et al. (2004). The similarity in the rheological property of olivine with a different Mg# may be worth mentioning for high-pressure rheological experiments using synthetic materials. The differential stress of $MgAl_2O_4$ spinel at 10 GPa used in this study also shows good agreement with data reported by Weidner et al. (2001).

During heating, thermally induced yielding occurred to relieve the differential stress. When the samples were

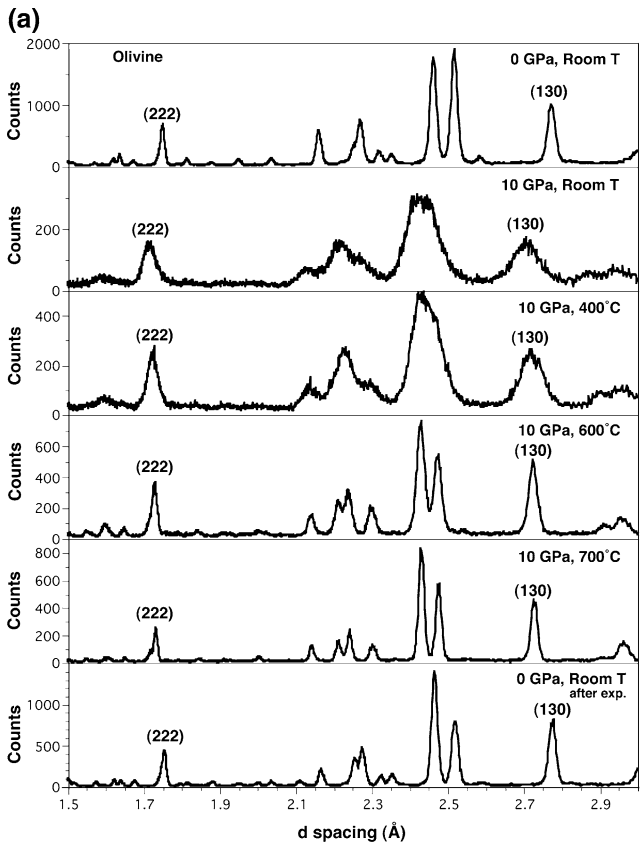
(a)
Olivine
0 GPa, Room T
(222)
(130)
10 GPa, Room T
10 GPa, 400˚C
10 GPa, 600˚C
10 GPa, 700˚C
0 GPa, Room T
after exp.
Counts
d spacing (Å)

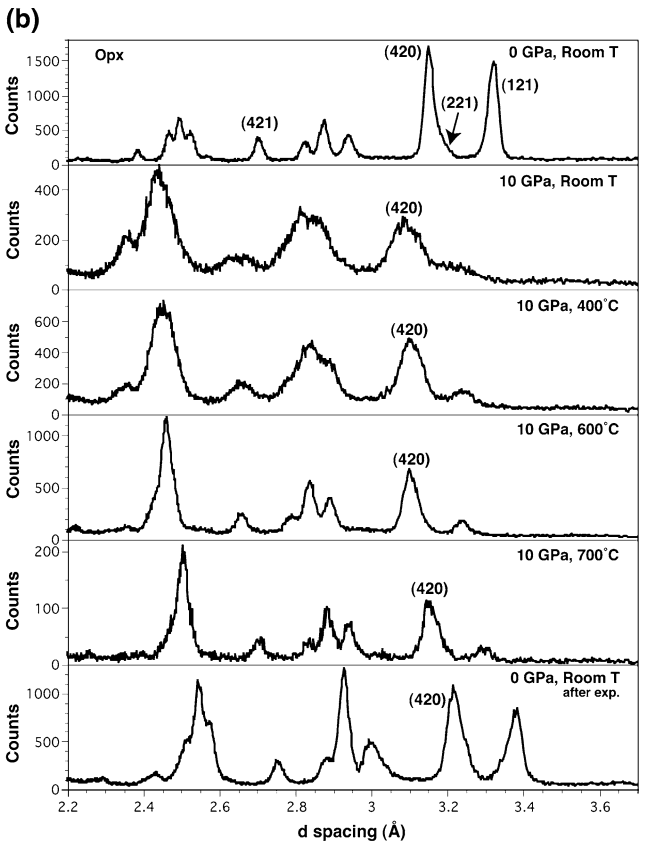
(b)
Opx
0 GPa, Room T
(420)
(421)
(221)
(121)
10 GPa, Room T
10 GPa, 400˚C
10 GPa, 600˚C
10 GPa, 700˚C
0 GPa, Room T
after exp.
Counts
d spacing (Å)

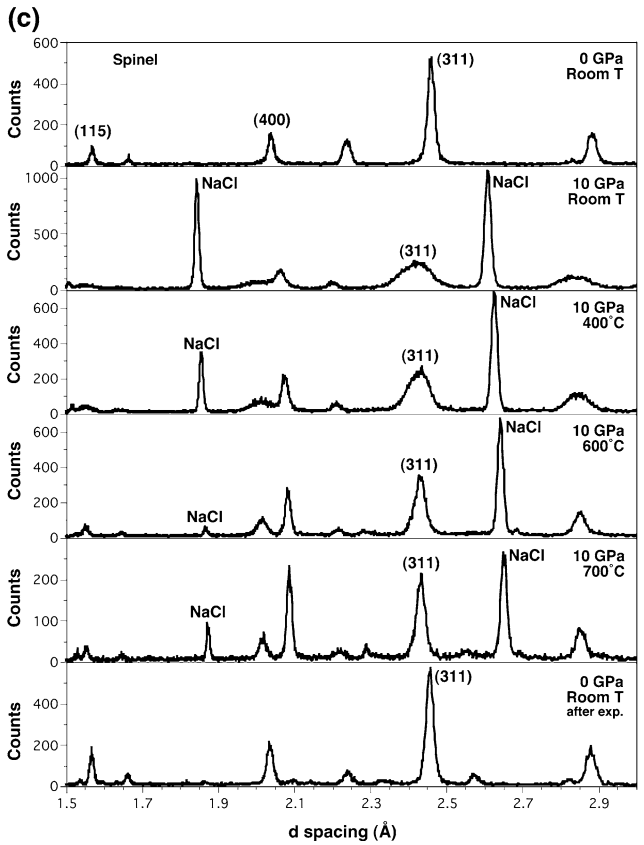
(c)
Spinel
0 GPa
Room T
(311)
(400)
(115)
NaCl
10 GPa
Room T
10 GPa
400˚C
10 GPa
600˚C
10 GPa
700˚C
0 GPa
Room T
after exp.
Counts
d spacing (Å)

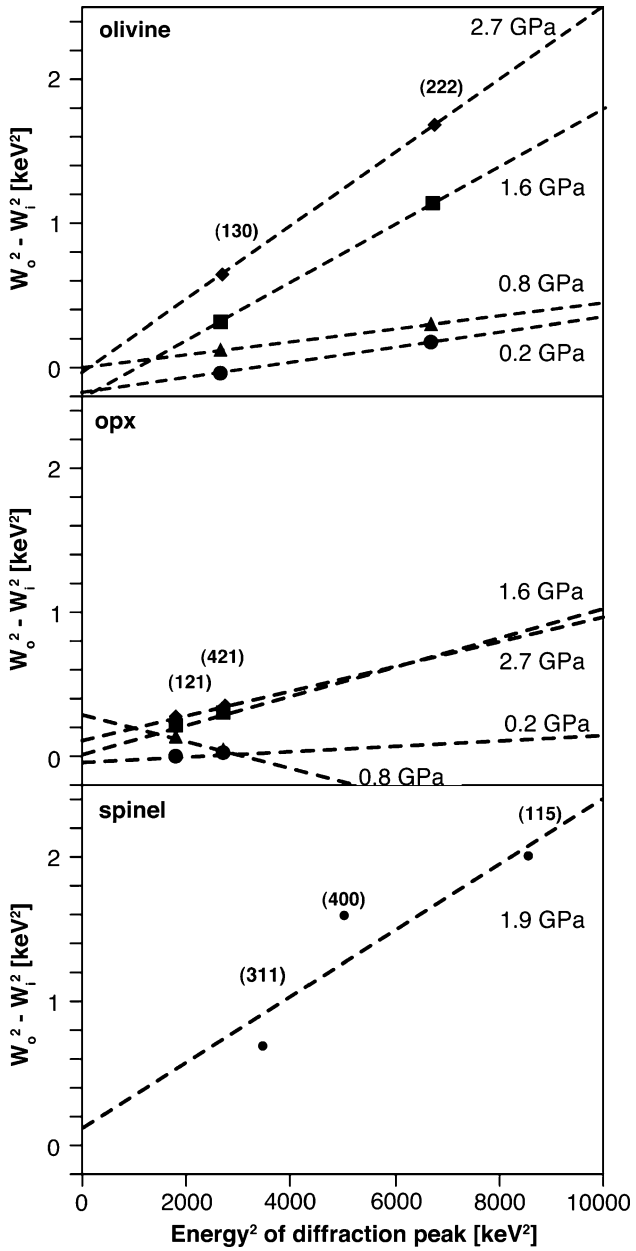

Fig. 4 Energy-dependent peak broadening for olivine, orthopyroxene, and spinel at room temperature. The unit of this figure is energy. Because Eq. (2) was derived from measured X-ray photon energy (Gerward et al. 1976)

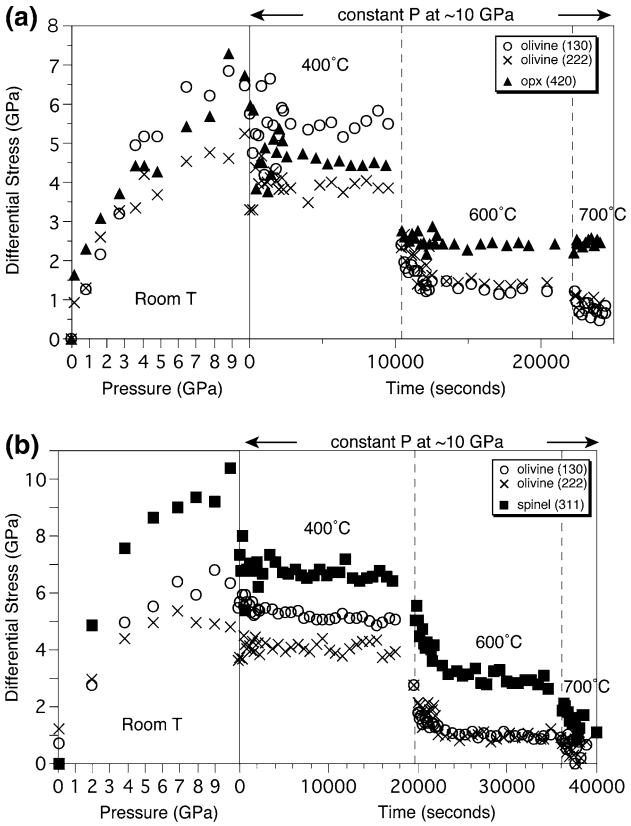

Fig. 5 Differential stress of samples as a function of the load pressure followed by heating at the constant load. Stresses calculated from different peaks are presented using different *symbols*: **a** shows olivine and orthopyroxene data, **b** shows data obtained through another relaxation experiment using a set of olivine and spinel

heated to 400°C, the differential stress started to decrease and finally reached an almost constant value (Fig. 5). At each temperature, the differential stresses for all minerals were similarly saturated at an approximately constant value, which can be considered as the yield strength of the sample at each temperature. No significant drop of differential stress is observed in olivine and orthopyroxene, but a slightly larger drop was observed in spinel at 400°C. The differential stresses of all minerals decrease drastically at 600°C. With additional heating at 700°C, the differential stress of olivine recovered to almost the same level as the starting value. Neither orthopyroxene nor spinel shows complete stress relaxation, but they apparently retain some stress even at 700°C. The differential stress of orthopyroxene (ca. 2 GPa) is greater than that of spinel (ca. 1.5 GPa), which indicates that orthopyroxene is stronger than olivine and spinel at a 10 GPa and 700°C condition.

Figure 6 shows the yield strength of the samples as a function of temperature. The yield strengths are estimated from the differential stresses in Fig. 5, which are values obtained at around 2,000 s after the samples were heated to each temperature. Olivine is the weakest at all temperature ranges. This result agrees with microstructural observations of mantle-derived peridotite, whose olivine grains deformed, rather than other constituent minerals such as orthopyroxene, clinopyroxene, and spinel (e.g., Sawaguchi and Ishii 2003). The present strengths of olivine are consistent with those reported by Chen et al. (1998) at the same P and T conditions. Although spinel is much stronger than orthopyroxene at less than 600°C, it becomes weaker at 700°C.

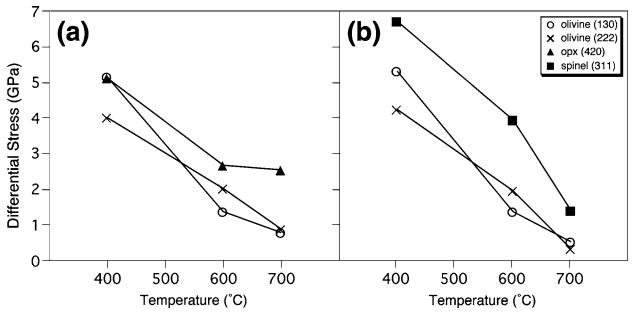

Fig. 6 Differential stress in samples as a function of temperature. The adopted stresses were obtaining by averaging three data of stresses at around 2,000 s after the temperature reached the value. Data of **a** and **b** are from Fig. 5a and b, respectively

The fluid inclusions existing in different minerals show different internal pressures, even in the same xenolith (De Vivo et al. 1988; Schwab and Freisleben 1988; Frezzotti et al. 1992; Yamamoto et al. 2002, 2007; Sapienza et al. 2005). The pressure mainly results from plastic deformation of the host mineral around the fluid inclusions that occur during depressurization, accompanied with transportation of the minerals to near the Earth's surface (Andersen and Neumann 2001; Yamamoto et al. 2002). The driving force of the plastic deformation is the pressure difference between the inside and outside of fluid inclusions. For example, in the case of a xenolith entrained by magma from 1 GPa (ca. 40 km depth) to the Earth's surface, the pressure difference between the inside and outside of fluid inclusions becomes 1 GPa. Here we emphasize that the stress induced by the pressure difference occurs only at a narrow surrounding part around the fluid inclusion; most of the crystal is under lithostatic conditions. Fluid inclusions in hard minerals such as a diamond must retain a constant pressure, even at the temperatures of typical basaltic magma (1,000–1,200°C), because plastic deformation does not occur efficiently around them (Weidner et al. 1994). On the other hand, the pressure reduction is probably greater in weaker minerals. Yamamoto et al. (2002) measured the residual pressure of fluid inclusions in olivine, orthopyroxene, and spinel. Those results suggest that the relative strength of these minerals is in the order of spinel $\geq$ orthopyroxene >> olivine at ca. 1 GPa and 950°C. This order is identical to that of the present result.

Our data present that the yield strengths of olivine, orthopyroxene, and spinel decrease with temperatures up to 700°C at 10 GPa. The progressive decrease in the yield strength is expected at a temperature greater than 700°C (Fig. 6). Li et al. (2007) reported that the yield strength of $MgAl_2O_4$ spinel is 3.83 GPa at 800°C with steady state creep of 3×10^{-5} s^{-1}; it dropped to 0.2 GPa at 1,000°C. Such a sharp drop in the yield strength with temperature resembles the characteristics of the spinel (311) used in this study. Regarding the pressure dependence of the yield strength, negative values of activation volume are not reported for olivine: 0–27 cm^3/mol (Ross et al. 1979; Green and Borch 1987; Kohlstedt and Wang 2001; Karato and Wu 1993; Li et al. 2004; 2006). This represents that the yield strength of olivine decreases with decreasing pressure. These facts indicate that the inner pressure of the fluid inclusion in xenolith entrained at ca. 1 GPa is fully relaxed in the basaltic magma. Indeed Karato and Jung (2003) reported a relationship between creep strength and pressure of olivine, indicating that dry olivine has a strength of only ca 0.3 GPa at pressure (0–1 GPa) and temperature of 1,300°C. However, the fluid inclusions in mantle-derived xenoliths retain the high-fluid density corresponding to around 0.8 GPa at 1,000°C, even in soft minerals such as olivine (e.g. Yamamoto et al. 2002, 2007). This discrepancy is explainable by the high-density of tangled dislocations that occur within several micrometers from the walls of fluid inclusions (Fig. 7). Tangling of dislocations is known as an important mechanism of work hardening, which is the strengthening of a material caused by accumulation of dislocations created by differential stress. Therefore, the observed tangled dislocations should indicate that the plastic deformation of host olivine was prevented around the fluid inclusions; consequently, the fluid inclusions retain high-pressure. It is possible that identical processes occurred with both orthopyroxene and spinel. Microstructural observation (e.g., using a transmission electron microscope) will enable us to examine the density and type of dislocation around fluid inclusion in orthopyroxene and spinel. Such rheological observations elucidate characteristics of work hardening and the real

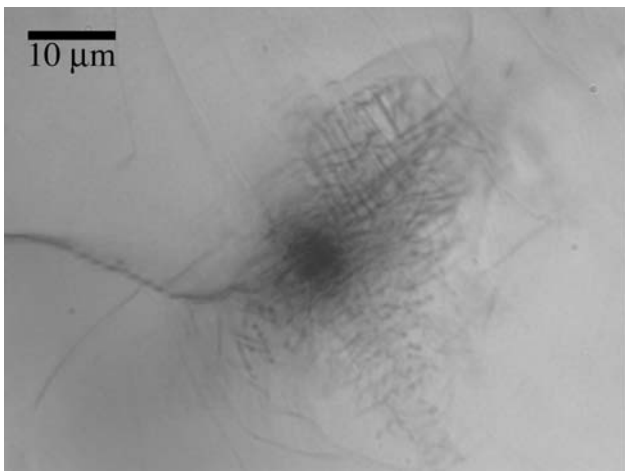

Fig. 7 Photomicrograph of olivine grain composed of the xenolith (En-1) treated using the oxidation-decoration method (Kohlstedt et al. 1975). Dense tangled dislocations are observed in olivine within several micrometers of the CO_2 fluid inclusion wall

strength of minerals surrounding fluid inclusion. They enable us to discuss the validity of fluid inclusions as probes for the depth scale and deformation mechanisms.

Conclusions

We compared yield strengths of natural mantle minerals (olivine, orthopyroxene, and spinel) by monitoring their X-ray diffraction patterns as a function of pressure, temperature, and time. Diffraction peaks broaden with increasing strain on compression to 10 GPa at room temperature, and then sharpen by plastic deformation during stepwise heating to 400, 600, and 700°C. Observations indicate that olivine is much weaker than the other two minerals throughout the range of conditions described above. That is, the yield strength of the natural mantle minerals is in the order of spinel $\approx$ orthopyroxene $>$ olivine. Differential stresses of all minerals dropped to less than 2 GPa at 700°C, suggesting that the yield strengths of the minerals drop to near zero at temperatures greater than ca. 800°C. Mantle-derived minerals often have fluid inclusions with high-fluid density corresponding to the original depth (ca. 40 km = ca. 1 GPa). There must be some mechanism to withstand the residual pressure. Possible work hardening around the inclusions caused by tangled dislocations might inhibit reduction of the residual pressure of fluid inclusions.

Acknowledgments Drs. Matsui M., Nishihara Y. and an anonymous reviewer provided thoughtful comments to improve the manuscript. We appreciate Y. Higo, F. Kurio, T. Sanehira, Y. Sueda and colleagues at Ehime University for their help in creating the pressure cell. This study was supported by a Grant-in-aid for the twenty-first Century COE Program for KAGI21 (Kyoto University, G3) and for Frontiers in Fundamental Chemistry, and by Grants-in-aid for Scientific Research (Nos. 13554018, 14654096, 15340190, 18740344 and 19GS0205) from the Japan Society for the Promotion of Science (JSPS) and JSPS Postdoctoral Fellowships for Research Abroad.

References

Anderson OL, Isaak DG (1995) Elastic constants of mantle minerals at high temperature. In: Ahrens TJ (ed) Mineral Physics & Crystallography, AGU Reference Shelf 2, pp 64–97

Andersen T, Neumann E-R (2001) Fluid inclusions in mantle xenoliths. Lithos 55:301–320

Bass JD (1995) Elasticity of minerals, glasses and melts In: Ahrens TJ (ed) Mineral Physics & Crystallography, AGU Reference Shelf 2, pp 45–63

Chen J, Inoue T, Weidner DJ et al (1998) Strength and water weakening of mantle minerals, olivine, wadsleyite and ringwoodite. Geophys Res Lett 25:575–578

Chen J, Weidner DJ, Vaughan MT (2002) The strength of $Mg_{0.9}Fe_{0.1}SiO_3$ perovskite at high pressure and temperature. Nature 419:824–826

Decker DL (1971) High-pressure equation of state for NaCl, KCl and CsCl. J Appl Phys 42:3239–3244

De Vivo B, Frezzotti ML, Lima A et al (1988) Spinel lherzolite nodules from Oahu Island (Hawaii): a fluid inclusion study. Bull Mineral 111:307–319

Frezzotti ML, Burke EAJ, DeVivo B et al (1992) Mantle fluids in pyroxenite nodules from Salt Lake Crater (Oahu, Hawaii). Eur J Mineral 4:1137–1153

Gerward L, Morup S, Topsoe H (1976) Particle size and strain broadening in energy-dispersive X-ray powder patterns. J App Phys 47:822–825

Green HW, Borch RS (1987) The pressure dependence of creep. Acta Metall 35:1301–1315

Hirano N, Yamamoto J, Kagi H et al (2004) Young olivine xenocryst-bearing alkali-basalt from the oceanward slope of the Japan Trench. Contrib Mineral Petrol 148:47–54

Hirth G, Kohlstedt D (2003) Rheology of the upper mantle and the mantle wedge: a view from the experimentalists. In: Eiler J (ed) Inside the subduction factory, J AGU Geophys Monogr 138:83–105

Irifune T (2002) Application of synchrotron radiation and Kawai-type apparatus to various studies in high-pressure mineral physics. Min Mag 66:769–790

Karato S-I, Wu P (1993) Rheology of the upper mantle a synthesis. Science 260:771–778

Karato S, Jung H (2003) Effects of pressure on high-temperature dislocation creep in olivine. Philos Mag 83:401–414

Kohlstedt DL, Wang Z (2001) Grain-boundary sliding accommodated dislocation creep in dunite. EOS Trans AGU 82:F1137

Kohlstedt DL, Goetze C, Durham WB et al (1975) A new technique for decorating dislocations in olivine. Science 191:1045–1046

Kung J, Li B, Uchida T et al (2004) In situ measurements of sound velocities and densities across the orthopyroxene—high-pressure clinopyroxene transition in $MgSiO_3$ at high pressure. Phys Earth Planet Int 147:27–44

Li L, Weidner D, Raterron P et al (2004) Stress measurements of deforming olivine at high pressure. Phys Earth Planet Int 143–144:357–367

Li L, Weidner D, Raterron P et al (2006) Deformation of olivine at mantle pressure using D-DIA. Eur J Mineral 18:7–19

Li L, Addad A, Weidner D et al (2007) High pressure deformation in two-phase aggregates. Tectonophysics 439:107–117

Mackwell SJ (1991) High-temperature rheology of enstatite: implications for creep in the mantle. Geophys Res Lett 18:2027–2030

Mitchell TE, Hwang L, Heuer AH (1976) Deformation in spinel. J Material Sci 11:264–272

Raterron P, Wu Y, Weidner DJ et al (2004) Low-temperature olivine rheology at high pressure. Phys Earth Planet Int 145:149–159

Roedder E (1965) Liquid CO_2 inclusions in olivine-bearing nodules and phenocrysts from basalts. Am Mineral 50:1746–1782

Ross JV, Ave Lallemant HG, Carter NL (1979) Activation volume for creep in the upper mantle. Science 203:261–263

Sapienza G, Hilton DR, Scribano V (2005) Helium isotopes in peridotite mineral phases from Hyblean Plateau xenoliths (southeastern Sicily, Italy). Chem Geol 219:115–129

Sawaguchi T, Ishii K (2003) Three-dimensional numerical modeling of lattice- and shape-preferred orientation of orthopyroxene porphyroclasts in peridotites. J Struct Geol 25:1425–1444

Saxena SK, Chatterjee N, Fei Y et al (1993) Thermodynamic data on oxides and silicates. Springer, New York

Schwab RG, Freisleben B (1988) Fluid CO_2 inclusions in olivine and pyroxene and their behaviour under high pressure and temperature conditions. Bull Mineral 111:297–306

Ulmer P, Stalder R (2001) The $Mg(Fe)SiO_3$ orthoenstatite-clinoenstatite transitions at high pressures and temperatures determined

by Raman-spectroscopy on quenched samples. Am Mineral 86:1267–1274

Utsumi W, Funakoshi K, Urakawa S et al (1998) SPring-8 beamlines for high pressure science with multi-anvil apparatus. Rev High Pressure Sci Technol 7:1484–1486

Weidner DJ (1998) Rheological studies at high pressure. In: Hemley RJ, Mao HK (eds) Ultrahigh-pressure mineralogy: physics and chemistry of the earth's deep interior. Mineralogical Society of America, Washington, DC, pp 493–524

Weidner DJ, Wang Y, Vaughan MT (1994) Yield strength at high pressure and temperature. Geophys Res Lett 21:753–756

Weidner DJ, Wang Y, Chen G et al (1998) Rheology measurements at high pressure and temperature. Geophys Monogr 101:473–482

Weidner DJ, Chen J, Xu Y et al (2001) Subduction zone rheology. Phys Earth Planet Int 127:67–81

Wells PRA (1977) Pyroxene thermometry in simple and complex systems. Contrib Mineral Petrol 62:129–139

Yamamoto J, Kagi H, Kaneoka I et al (2002) Fossil pressures of fluid inclusions in mantle xenoliths exhibiting rheology of mantle minerals: implications for the geobarometry of mantle minerals using micro Raman spectroscopy. Earth Planet Sci Lett 198:511–519

Yamamoto J, Kaneoka I, Nakai S et al (2004) Evidence for subduction-related components in the subcontinental mantle from low $^{3}He/^{4}He$ and $^{40}Ar/^{36}Ar$ ratio in mantle xenoliths from Far Eastern Russia. Chem Geol 207:237–259

Yamamoto J, Kagi H, Kawakami Y et al (2007) Paleo-Moho depth determined from the pressure of CO_2 fluid inclusions: Raman spectroscopic barometry of mantle- and crust-derived rocks. Earth Planet Sci Lett 253:369–377

Zhang J, Wang L, Weidner DJ et al (2002) The strength of moissanite. Am Mineral 87:1005–1008